REVISTA INTERDISCIPLINAR DE PESQUISA EM ENGENHARIA

CILAMCE 2016

XXXVII IBERIAN LATIN AMERICAN CONGRESS ON COMPUTATIONAL METHODS IN ENGINEERING
BRASÍLIA - DF - BRAZIL

A PHENOMENOLOGICAL INTERNAL VARIABLE MODELING OF HIGH-STRAIN-RATE COLD DEFORMATION OF FCC METALS

Tiago dos Santos

Rodrigo Rossi

tsantos.mec@gmail.com

rrossi@ufrgs.br

UFRGS/DEMEC/PROMEC

425, Sarmento Leite, 90.050-170, Porto Alegre, RS, Brazil

Pedro A. R. Rosa

pedro.rosa@tecnico.ulisboa.pt

ULISBOA/IST/IDMEC

01, Rovisco Pais, 1049-001, Lisbon, Portugal

Samir Maghous

samir.maghous@ufrgs.br

UFRGS/DECIV/PPGEC

99, Osvaldo Aranha, 90.035-190, Porto Alegre, RS, Brazil

Abstract. In this work a macroscopic viscoplastic model, accounting for strain, strain rate hardening and instantaneous rate sensitivity of FCC metals, is formulated. Within the present approach, a single phenomenological internal variable representing an effective microstructural feature is introduced. In a phenomenological way, this internal variable is related to hardening mechanisms associated with large strain processes. Aiming at applying the constitutive proposal in solving engineering problems, associated numerical formulation is also described. Reasoning on the numerical context, an exponential implicit integration scheme is adopted together with an elastic predictor-plastic corrector algorithm. Constitutive capabilities are assessed by solving simple numerical problems involving high-strain-rate deformation. Simulation results

and comparisons with experimental data available in the literature, considering an annealed high purity copper, demonstrate the model aptitude in predicting strain rate history effects on material response. In general, proposed model proves to be a useful modeling alternative to describe the macroscopic behavior of FCC metals subjected to high-strain-rate cold deformation.

Keywords: *High strain rate effects, Finite strains, Viscoplasticity, Numerical algorithms*

1 INTRODUCTION

Nowadays, several engineering applications, such as high speed forming and machining of metals, analysis of structural crashworthiness in the automotive and aerospace industries, military and defence activities, involve high strain rates and large strain deformation processes. Considering these applications, to properly predict the material behavior under extreme conditions, as high velocity and large strains, a constitutive model have to consider loading history effects. For example, the hardening response of FCC metals is strongly rate-dependent at high velocity conditions (Klepaczko, 1975; Chiem and Duffy, 1983; Tanner and McDowell, 1999; Huang and Tao, 2011; Luo et al., 2012). However, a constitutive formulation to solve engineering problems should incorporate proper constitutive capabilities, while keeping its simplicity in order to save computational efforts. On one hand, physically-based approaches (Follansbee and Kocks, 1988; Klepaczko, 1988; Voyiadjis and Almasri, 2008; Gao and Zhang, 2012; Rodríguez-Martínez et al., 2011) can provide detailed constitutive descriptions considering loading history effects by means of dislocation density evolution equations. On the other hand, physical formulations increase the model complexity and the number of constants to be adjusted (see e.g. discussion of Rusinek and Jankowiak (2014)). Therefore, reasoning on model simplicity, with the aim of providing constitutive approaches containing lower number of material constants, and thus requiring less experiments to identify these parameters, many researchers (Bodner and Rubin, 1994; Molinari and Ravichandran, 2005; Durrenberger et al., 2008; Rodríguez-Martínez et al., 2009) have proposed phenomenological (or semi-physical) models. Toward this objective, dos Santos et al. (2016b) recently proposed a simplified viscoplastic model, which provided good correlations with high strain rate experiments of an annealed OFHC copper.

As already mentioned, in order to guarantee appropriate predictions and to save computational time, engineering simulations require accurate, efficient, and robust numerical tools. The finite element (FE) method has been widely employed in solving nonlinear initial boundary value problems (Simo and Hughes, 1998; de Souza Neto et al., 2008). However, to integrate a local constitutive model within a FE framework, the update of stress and state variables from a given strain increment, and the calculation of consistent tangent modulus have to be carried out (Simo and Hughes, 1998; de Souza Neto et al., 2008). Aiming at accomplishing these tasks and improving the computational efficiency, several viscoplastic implicit integration algorithms for large strain problems have been proposed (Lush et al., 1989; Weber and Anand, 1990; Zaera and Fernández-Sáez, 2006; Mourad et al., 2014). Specifically, Lush et al. (1989) proposed a time-integration procedure for implementing the model of Anand (1985) into a displacement-based FE context. Zaera and Fernández-Sáez (2006) implemented the constitutive model of Rusinek and Klepaczko (2001) exploring both overstress (Perzyna, 1966, 1971) and consistency (Wang et al., 1997) vicoplastic models. Mourad et al. (2014) proposed an integration scheme in order to incorporate the *MTS* model of Follansbee and Kocks (1988) into a FE framework. In order to numerically investigate strain rate hardening effects on FCC metals, dos Santos et al. (2016a) employed the previously proposed viscoplastic model (dos Santos et al., 2016b) in high strain rate simulations. In general, mostly of the large strain formulations are based on the well-known multiplicative decomposition of the deformation gradient (Lee, 1969; Mandel, 1972), and generally associated algorithmic formulations preserves material objectivity.

The present work aims in summarizing and exploring the main modeling results obtained in previous researches concerning high strain rate deformation processes (dos Santos et al., 2016b,a). The whole constitutive approach consists of a simple and robust modeling framework

to account for strain, strain-rate hardening and viscous response of FCC metals under high strain rate straining. Constitutive formulation adopts a *von Mises* plasticity considering a strain-rate-dependent isotropic hardening whose evolution follows the *overstress* framework of Perzyna (1966, 1971). In the present approach, the isotropic hardening is given as an evolution results of a single scalar internal variable describing an effective microstructural feature (Molinari and Ravichandran, 2005; dos Santos et al., 2016b). The stress hardening variable is composed by two uncoupled contributions: A_1 and A_2. The first can be qualitatively associated with dislocations accumulation processes. The second contribution, A_2, can be related to hardening mechanisms responsible for the deformation Stage IV, in which the main hardening contribution is due to strain-induced granular misorientations.

As commented earlier, the continuum formulation to be employed in this work is based on the viscoplastic model proposed in (dos Santos et al., 2016b). In addition, adopted numerical approach (dos Santos et al., 2016a) follows a total *Lagrangian* description, considering the classical multiplicative decomposition of the deformation gradient. Furthermore, a fully isotropic material is considered, whose constitutive formulation stated in terms of the *Hencky* (logarithmic) deformation and the rotated *Kirchhoff* (or *Mandel*) stress. Concerning the reversible behavior, a linear hyperelastic response is assumed. In addition, following the works of Eterovic and Bathe (1990) and Weber and Anand (1990), an exponential implicit integration scheme is adopted. Related nonlinear equations are solved by using an elastic predictor-plastic corrector algorithm. Therefore, adopted numerical strategy furnishes incremental elastic-viscoplastic solution associated with each reversible or irreversible deformation increment.

The work is organized as follows. Section 2 presents an overview of the constitutive model adopted (dos Santos et al., 2016b). Section 3 outlines the local incremental constitutive formulation, recalling the elastic predictor-plastic corrector algorithm. In Sec. 4, in order of demonstrating model aptitude, and exploring constitutive descriptions associated with loading history effects, some numerical simulations are performed: namely a decremental strain rate testing and a constant strain rate loading followed by stress relaxation. These simulations consider the model parameters obtained by dos Santos et al. (2016b) considering an annealed OFHC copper. Numerical results are compared with experimental data available in the literature (Tanner and McDowell, 1999; Jordan et al., 2013), from these comparisons good correlations are observed. The work is closed with conclusions and comments in Sec. 5.

2 CONSTITUTIVE FORMULATION

We adopt the multiplicative[1] decomposition of the deformation gradient (Lee, 1969; Mandel, 1973)

$$\boldsymbol{F} = \boldsymbol{F}^e \boldsymbol{F}^{vp}, \tag{1}$$

where $\boldsymbol{F} = \frac{\partial \boldsymbol{\varphi}(\boldsymbol{X},t)}{\partial \boldsymbol{X}}$, $\boldsymbol{\varphi}$ is the displacement function mapping an initial point $\boldsymbol{X} \in \Omega_0$ onto a current one $\boldsymbol{x} \in \Omega$ at time t, i.e. $\boldsymbol{x} = \boldsymbol{\varphi}(\boldsymbol{X}, t)$. Terms $\boldsymbol{F}^e$ and $\boldsymbol{F}^{vp}$ are the elastic and viscoplastic part of $\boldsymbol{F}$. Adopting decomposition (1), the specific *Helmholtz* free-energy can be split (Lubliner, 1984),

$$\psi = \psi^e\left(\boldsymbol{E}^e\right) + \psi^{vp}\left(\alpha\right), \tag{2}$$

[1] Along this work single contractions between second-order tensors are omitted, i.e., $\boldsymbol{S}\cdot\boldsymbol{T} = \boldsymbol{S}\boldsymbol{T}$, in components $\left(\boldsymbol{S}\boldsymbol{T}\right)_{ij} = S_{ik}T_{kj}$.

into its elastic ψ^e and inelastic ψ^{vp} parts. Tensor $\boldsymbol{E}^e = \ln(\boldsymbol{U}^e)$ is the *Hencky* elastic strain with $\boldsymbol{U}^{e^2} = (\boldsymbol{F}^e)^T \boldsymbol{F}^e$ and $\boldsymbol{F}^e = \boldsymbol{F}\boldsymbol{F}^{vp^{-1}}$. A single internal variable α is assumed to describe irreversible material behavior (see for instance references (Coleman and Gurtin, 1967; Rice, 1971; Lubliner, 1972, 1984)). In this work we assume standard quadratic forms

$$\psi^e = \frac{1}{2}\boldsymbol{E}^e : \mathbb{D}^e : \boldsymbol{E}^e \text{ and } \psi^{vp} = \frac{1}{2}H\alpha^2, \tag{3}$$

where $\mathbb{D}^e$ is a symmetric positive-definite forth-order elastic tensor and $H \geq 0$ is the hardening modulus. Furthermore, isotropic elasticity is considered in subsequent analysis:

$$\mathbb{D}^e = 2\mu\mathbb{I} + \left(\kappa - \frac{2}{3}\mu\right)\boldsymbol{I} \otimes \boldsymbol{I}, \tag{4}$$

where $\mathbb{I}$, $\boldsymbol{I}$, μ and κ are the fourth-order and the second-order identity tensors, the shear and bulk modulus, respectively. Components of $\mathbb{I}$ are $I_{ijkl} = \frac{1}{2}(\delta_{ik}\delta_{jl} + \delta_{il}\delta_{jk})$ with δ_{ij} denoting the *Kronecker*'s symbol.

Associated thermodynamic forces obey the constitutive equations

$$\bar{\boldsymbol{\tau}} = \rho_0 \frac{\partial \psi^e}{\partial \boldsymbol{E}^e} = \mathbb{D}^e : \boldsymbol{E}^e \text{ and } A = \rho_0 \frac{\partial \psi^{vp}}{\partial \alpha} = H\alpha, \tag{5}$$

being $\bar{\boldsymbol{\tau}}$ the rotated *Kirchhoff* stress (Eterovic and Bathe, 1990), which is related to the *Kirchhoff* stress tensor $\boldsymbol{\tau}$ by means of the right rotation tensor $\boldsymbol{R} = \boldsymbol{F}\boldsymbol{U}^{-1}$ with $\boldsymbol{U}^2 = \boldsymbol{F}^T\boldsymbol{F}$, such that $\bar{\boldsymbol{\tau}} = \boldsymbol{R}^T\boldsymbol{\tau}\boldsymbol{R}$. In addition, $\boldsymbol{\tau}$ and the *Cauchy* stress tensor $\boldsymbol{\sigma}$ are related through $\boldsymbol{\tau} = J\boldsymbol{\sigma}$ with $J = \det(\boldsymbol{F})$. Parameter A stands for the isotropic hardening associated with α. In what follows, a *von Mises* yield criterion, together with an isotropic hardening A, is adopted

$$f(\bar{\boldsymbol{\tau}}, A) = \left\|\bar{\boldsymbol{\tau}}^D\right\| - \sqrt{\frac{2}{3}}(\sigma_y + A), \tag{6}$$

in which $\left\|\bar{\boldsymbol{\tau}}^D\right\| = \sqrt{\bar{\tau}^D_{ij}\bar{\tau}^D_{ij}}$, $\bar{\boldsymbol{\tau}}^D = \bar{\boldsymbol{\tau}} - \frac{1}{3}\mathrm{tr}(\bar{\boldsymbol{\tau}})\boldsymbol{I}$ is the deviatoric part of $\bar{\boldsymbol{\tau}}$ and σ_y is the initial yield stress.

2.1 Evolution equations

The viscoplastic strain rate $\bar{\boldsymbol{D}}^{vp} = \mathrm{sym}\left(\dot{\boldsymbol{F}}^{vp}\boldsymbol{F}^{vp^{-1}}\right)$ follows an associative evolution,

$$\bar{\boldsymbol{D}}^{vp} = \dot{\lambda}\frac{\partial f}{\partial \bar{\boldsymbol{\tau}}} \tag{7}$$

where the viscoplastic multiplier $\dot{\lambda}$ is given by (Perzyna, 1966, 1971)

$$\dot{\lambda} = \frac{1}{\vartheta}\Theta(\langle f \rangle, A). \tag{8}$$

In the above constitutive relation, operator $\langle x \rangle \equiv \frac{1}{2}(x + |x|)$ denotes the *Macaulay* brackets, $\vartheta \geq 0$ is the material viscosity parameter and $\Theta \geq 0$ is a convex *overstress* function of both f and A. Hardening variable A is given by

$$A = A_1 + cA_\infty\varepsilon, \tag{9}$$

where $c \geq 0$ is a material constant, A_∞ is the work hardening saturation, A_1 can be associated with hardening induced by dislocation storage, and term $cA_\infty\varepsilon$ can be related to geometric

hardening due to strain-induced misorientations. Evolution of A_1 is given by

$$\dot{A}_1 = H_1 \left(1 - \frac{A_1}{A_\infty}\right) \dot{\varepsilon}, \tag{10}$$

where H_1 is the hardening rate and

$$\dot{\varepsilon} = \sqrt{\frac{2}{3}} \left\| \bar{\boldsymbol{D}}^{vp} \right\| \geq 0 \tag{11}$$

is the accumulated viscoplastic strain rate. Considering a constant rate $\dot{\varepsilon}$, Eq. (10) is directly integrated, yielding a *Voce* hardening law (Voce, 1948),

$$\frac{A_1 - A_\infty}{A_{1_i} - A_\infty} = \exp\left[-\delta\left(\varepsilon - \varepsilon_i\right)\right]. \tag{12}$$

Parameters A_{1_i} and ε_i are initial values associated with A_1 and ε, respectively. In the present formulation we assume a constant ratio $\delta = \frac{H_1}{A_\infty}$, and a rate dependence is assigned to A_∞. Combining Eqs. (9) and (12), we have

$$A = A_i + A_\infty c\left(\varepsilon - \varepsilon_i\right) + \left[A_\infty\left(1 + c\varepsilon_i\right) - A_i\right]\left\{1 - \exp\left[-\delta\left(\varepsilon - \varepsilon_i\right)\right]\right\}, \tag{13}$$

where A_i is the initial hardening. Considering that $A_i = \varepsilon_i = 0$, a reduced version of Eq. (13) is obtained,

$$A = A_\infty\left[1 + c\varepsilon - \exp\left(-\delta\varepsilon\right)\right], \tag{14}$$

which can be seen as a modified *Voce* hardening rule. Hardening equation (13), obtained based upon the assumption of constant rate $\dot{\varepsilon}$, is usefull to be employed modeling constant strain rate loading processes. Concerning rate-dependence of parameter A_∞, the following relation is adopted (see dos Santos et al. (2016b)):

$$A_\infty = \left[1 - \beta\left(\dot{\varepsilon}\right)\right] A_\infty^{lwr} + \beta\left(\dot{\varepsilon}\right) A_\infty^{up}, \tag{15}$$

where A_∞^{lwr} is the *quasi*-static hardening saturation measured at a lower reference strain rate $\dot{\varepsilon}_{lwr} \ll 1$ and A_∞^{up} is the value associated with an upper reference rate $\dot{\varepsilon}_{up} \gg 1$. A functional form of β satisfying $\beta\left(\dot{\varepsilon}_{lwr}\right) = 0$ and $\beta\left(\dot{\varepsilon}_{up}\right) = 1$ is adopted,

$$\beta\left(\dot{\varepsilon}\right) = \left(\frac{\dot{\varepsilon} - \dot{\varepsilon}_{lwr}}{\dot{\varepsilon}_{up} - \dot{\varepsilon}_{lwr}}\right)^{\xi}, \tag{16}$$

in which $\xi > 0$ is a material constant.

In the present approach, an overstress function $\Theta\left(\langle f \rangle, A\right)$ based on that proposed by Perić (1993) is adopted,

$$\vartheta\dot{\lambda} = \Theta\left(\langle f \rangle, A\right) = \left(\frac{\langle f \rangle + R}{R}\right)^{m} - 1. \tag{17}$$

Considering this function for $f \geq 0$, the inversion with respect to $\dot{\lambda}$ and f yields

$$f = \Theta^{-1}\left(\dot{\lambda}, A\right) = R\left[\left(1 + \vartheta\dot{\lambda}\right)^{\frac{1}{m}} - 1\right], \tag{18}$$

in which $\frac{1}{m}$ is the rate sensitivity parameter and $R(A)$ is a characteristic size of the elastic domain. Considering the *von Mises* yield criterion of Eq. (6), we have

$$R(A) = \sqrt{\frac{2}{3}}(\sigma_y + A). \tag{19}$$

2.2 Analytical constitutive descriptions

At this point, before going ahead, we summarize the constitutive formulation considering a rigid-viscoplastic material subjected to uniaxial stress state imposed in a constant rate loading ($\dot{\varepsilon} = \text{cte}$). This simplification is carried out in order to readily provide a reduced uniaxial stress model and to highlight analytical constitutive features associated with the present formulation. Therefore, from Eqs. (6), (18), by assuming a uniaxial stress $\bar{\tau}_{11}$ the following reduced equation is obtained (see dos Santos et al. (2016b)):

$$|\bar{\tau}_{11}| = (\sigma_y + A)\left(1 + \sqrt{\frac{3}{2}}\vartheta\dot{\varepsilon}\right)^{\frac{1}{m}}. \tag{20}$$

In which, in view of Eq. (14), we have

$$A = A_\infty\left[1 + c\varepsilon - \exp(-\delta\varepsilon)\right], \tag{21}$$

where, from Eqs. (15) and (16), saturation parameter is given by

$$A_\infty = A_\infty^{lwr} + \left(\frac{\dot{\varepsilon} - \dot{\varepsilon}_{lwr}}{\dot{\varepsilon}_{up} - \dot{\varepsilon}_{lwr}}\right)^{\xi}\left(A_\infty^{up} - A_\infty^{lwr}\right). \tag{22}$$

Table 1: Material properties and model parameters associated with annealed OFHC copper (dos Santos et al., 2016b).

E	ν	σ_y	δ	c	A_∞^{lwr}	A_∞^{up}	$\dot{\varepsilon}_{lwr}$	$\dot{\varepsilon}_{up}$	ξ	ϑ	m
[GPa]	[–]	[MPa]	[–]	[–]	[MPa]	[MPa]	$[\text{s}^{-1}]$	$[\text{s}^{-1}]$	[–]	[s]	[–]
112	0.33	35	6.46	0.42	233	420	10^{-4}	10^{4}	3.16	1.2×10^{3}	105

Reasoning on this reduced uniaxial stress model, we adopt material parameters obtained by dos Santos et al. (2016b) using experimental results[2] of an annealed OFHC copper (Nemat-Nasser and Li, 1998; Tanner and McDowell, 1999; Jordan et al., 2013). Those material parameters are given in Tab. 1. Then, reasoning on the reduced model of Eqs. (20)-(22) and parameters of Tab. 1, flow stress can be calculated as an explicit function of both strain ε and strain rate $\dot{\varepsilon}$, as can be seen in Fig. 1(a). Assuming a given strain level of $\varepsilon = 0.2$, the flow stress rate-sensitivity is shown in Fig. 1(b), where the model flow stress curve ($|\bar{\tau}_{11}|$ v.s. $\dot{\varepsilon}$) is also compared with experimental data of Jordan et al. (2013). Furthermore, in order to demonstrate the strain rate influence on the hardening response, in Fig. 1(b) the yield stress curve $\left(\sigma_y + A \text{ v.s. } \dot{E}_{11}\right)$ is also displayed. In this figure, up to strain rates close to $10^3\,\text{s}^{-1}$ the *quasi*-static strength $(\sigma_y + A)$

[2]Experiments report true stress-true strain curves. However, assuming a rigid-viscoplastic material under a simple tensile/compression testing, the uniaxial *Cauchy* stress σ_{11} and rotated *Kirchhoff* stress $\bar{\tau}_{11}$ measures are coincident.

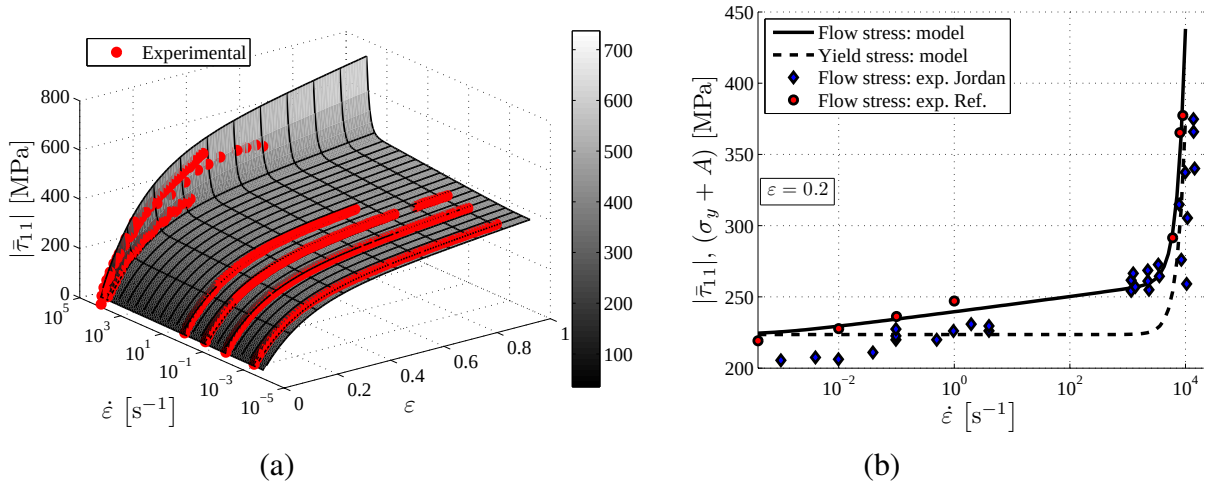

(a) (b)

Figure 1: (a) Model flow stress is terms of $(\varepsilon, \dot{\varepsilon})$ compared with reference experimental data; (b) Model rate-sensitivities for $\varepsilon = 0.2$ compared with reference experimental data (Ref.) and those of Jordan et al. (2013) (Jordan).

is practically rate-independent and for strain rates exceeding $10^3\,\mathrm{s}^{-1}$ it becomes strongly rate-dependent. This behavior can be attributed to a strong microstructural strain rate-sensitivity at high strain rates. Both Figs. 1(a) and 1(b) indicate the present model is able of accounting for the flow stress upturn strain rates within $10^3 - 10^4\,\mathrm{s}^{-1}$, and it fits well with data of Tanner and McDowell (1999). In addition, Fig. 1(b) also indicates the model description are in qualitative agreement with experiments of Jordan et al. (2013). The discrepancy between experiments of Tanner and McDowell (1999) and of Jordan et al. (2013), observed at low strain rates, can be due to different initial grain sizes and to inertia effects associated with specimen sizes (Jordan et al., 2013).

3 NUMERICAL FORMULATION

This section outlines the return mapping algorithm used in the resolution of the local equations. A standard finite strain elastic predictor-plastic corrector algorithm (Eterovic and Bathe, 1990; Weber and Anand, 1990) is extended in order to accommodate strain-rate-hardening effects within the numerical formulation.

3.1 Elastic predictor-plastic corrector algorithm

The elastic prediction phase assumes a fully elastic deformation increment, in which

$$\dot{\boldsymbol{F}}^{vp} = \mathbf{0} \;\text{ and }\; \dot{\alpha} = 0, \tag{23}$$

consequently

$$\boldsymbol{F}_{n+1}^{vp^{trial}} = \boldsymbol{F}_{n}^{vp} \;\text{ and }\; \alpha_{n+1}^{trial} = \alpha_n. \tag{24}$$

From these assumption, the *trial elastic state* is defined according to elastic deformation and associated logarithmic strain

$$\boldsymbol{F}_{n+1}^{e^{trial}} = \boldsymbol{F}_{n+1}\left(\boldsymbol{F}_{n+1}^{vp^{trial}}\right)^{-1} \quad \rightarrow \quad \boldsymbol{E}_{n+1}^{e^{trial}} = \frac{1}{2}\ln\left(\boldsymbol{C}_{n+1}^{e^{trial}}\right), \tag{25}$$

where $\boldsymbol{C}^{e^{trial}}_{n+1} = \left(\boldsymbol{F}^{e^{trial}}_{n+1}\right)^T \boldsymbol{F}^{e^{trial}}_{n+1}$. By knowing $\boldsymbol{E}^{e^{trial}}_{n+1}$, the trial-rotated *Kirchhoff* stress tensor is computed from Eq. (4): $\bar{\boldsymbol{\tau}}^{trial}_{n+1} = \bar{\boldsymbol{\tau}}^{trial}_{n+1}\left(\boldsymbol{E}^{e^{trial}}_{n+1}\right)$.

Return mapping step is required when $f\left(\bar{\boldsymbol{\tau}}^{trial}_{n+1}, A^{trial}_{n+1}\right) > 0$. In this work, an implicit exponential mapping is employed (Eterovic and Bathe, 1990; Weber and Anand, 1990), from which discretization of the plastic flow $\dot{\boldsymbol{F}}^{vp} = \bar{\boldsymbol{D}}^{vp}\boldsymbol{F}^{vp}$ follows

$$\boldsymbol{F}^{vp}_{n+1} = \exp\left(\Delta\lambda \boldsymbol{N}_{\bar{\boldsymbol{\tau}}_{n+1}}\right)\boldsymbol{F}^{vp}_{n}, \tag{26}$$

where $\boldsymbol{N}_{\bar{\boldsymbol{\tau}}_{n+1}} = \frac{\partial f_{n+1}}{\partial \bar{\boldsymbol{\tau}}_{n+1}} = \frac{\bar{\boldsymbol{\tau}}^{D}_{n+1}}{\left\|\bar{\boldsymbol{\tau}}^{D}_{n+1}\right\|}$. Equation (26) after some manipulations reduces to (Eterovic and Bathe, 1990; Weber and Anand, 1990)

$$\boldsymbol{E}^{e}_{n+1} = \boldsymbol{E}^{e^{trial}}_{n+1} - \Delta\lambda \boldsymbol{N}_{\bar{\boldsymbol{\tau}}_{n+1}}. \tag{27}$$

It is worth mentioning that when the constitutive formulation is restricted to elastic and inelastic isotropy, equivalence of Eqs. (26) and (27) is exact. Otherwise, passage is an approximation based on moderately small elastic deformation with a second-order error on elastic strains. These conditions are needed in order to obtain the relation $\boldsymbol{R}^{e}_{n+1} = \boldsymbol{R}^{e^{trial}}_{n+1}$, where $\boldsymbol{R}^{e} = \boldsymbol{F}^{e}\boldsymbol{U}^{e^{-1}}$ is the elastic right rotation tensor, and $\boldsymbol{U}^{e^2} = \boldsymbol{F}^{e^T}\boldsymbol{F}^{e}$ (Eterovic and Bathe, 1990; Weber and Anand, 1990).

Accumulated viscoplastic strain evolution, introduced in Eq. (11), is integrated following a backward *Euler* method,

$$\varepsilon_{n+1} = \varepsilon_n + \sqrt{\frac{2}{3}}\Delta\lambda. \tag{28}$$

In the last equation, multiplier $\Delta\lambda$ must satisfy

$$f\left(\bar{\boldsymbol{\tau}}_{n+1}, A_{n+1}\right) = \bar{\Theta}^{-1}\left(\Delta\lambda, A_{n+1}\right), \tag{29}$$

where $\bar{\Theta}^{-1}$ is the inverse function of $\bar{\Theta}$ in terms of f_{n+1} and $\Delta\lambda$. Function $\bar{\Theta}$ is the algorithmic version of Θ given in Eq. (17). To compute the hardening evolution considering Eqs. (10) and (9), a constant rate $\dot{\varepsilon} \approx \frac{\varepsilon_{n+1}-\varepsilon_n}{\Delta t}$ is assumed within time step $(t_n, t_{n+1}]$. Then, Eq. (13) can be used considering t_n as the initial state and t_{n+1} as the current time, what yields

$$A_{n+1} = A_n + A_{\infty_{n+1}} c\Delta\varepsilon_{n+1} + \left[A_{\infty_{n+1}}\left(1 + c\varepsilon_n\right) - A_n\right]\left[1 - \exp\left(-\delta\Delta\varepsilon_{n+1}\right)\right], \tag{30}$$

where $\Delta\varepsilon_{n+1} = \varepsilon_{n+1} - \varepsilon_n$, and by virtue of Eq. (15)

$$A_{\infty_{n+1}} = \left(1 - \beta_{n+1}\right) A^{lwr}_{\infty} + \beta_{n+1} A^{up}_{\infty}, \tag{31}$$

with (see Eq. (16))

$$\beta_{n+1} = \left[\frac{1}{\Delta t}\left(\frac{\varepsilon_{n+1} - \varepsilon_n - \Delta t\dot{\varepsilon}_{lwr}}{\dot{\varepsilon}_{up} - \dot{\varepsilon}_{lwr}}\right)\right]^{\xi}. \tag{32}$$

The return mapping algorithm consists therefore in determining the solution to nonlinear system of equations (27)-(32) with respect to the set of unknowns $\left\{\boldsymbol{E}^{e}_{n+1}, \varepsilon_{n+1}, \Delta\lambda, A_{n+1}, A_{\infty_{n+1}}, \beta_{n+1}\right\}$. However, equality $\boldsymbol{N}_{\bar{\boldsymbol{\tau}}_{n+1}} = \boldsymbol{N}_{\bar{\boldsymbol{\tau}}^{trial}_{n+1}}$ can be established in the context of *von Mises* criterion stated in Eq. (6). Equations (27)-(28) thus reduce to the single scalar equation:

$$\left\|\bar{\boldsymbol{\tau}}^{D^{trial}}_{n+1}\right\| - \Delta\lambda 2\mu - \sqrt{\frac{2}{3}}\left(\sigma_y + A_{n+1}\right) = \bar{\Theta}^{-1}\left(\Delta\lambda, A_{n+1}\right), \tag{33}$$

with unknowns $\Delta\lambda$ and A_{n+1}. Furthermore, inserting Eq. (28) into Eq. (30) yields

$$A_{n+1} = A_n + A_{\infty_{n+1}} c\sqrt{\frac{2}{3}}\Delta\lambda + \left[A_{\infty_{n+1}}\left(1 + c\varepsilon_n\right) - A_n\right]\left[1 - \exp\left(-\delta\sqrt{\frac{2}{3}}\Delta\lambda\right)\right], \quad (34)$$

while substituting Eqs. (28) and (32) into Eq. (31) gives

$$A_{\infty_{n+1}} = A_\infty^{lwr} + \left[\frac{1}{\Delta t}\left(\frac{\sqrt{\frac{2}{3}}\Delta\lambda - \Delta t\dot{\varepsilon}_{lwr}}{\dot{\varepsilon}_{up} - \dot{\varepsilon}_{lwr}}\right)\right]^{\xi}\left(A_\infty^{up} - A_\infty^{lwr}\right). \quad (35)$$

Then, the reduced return mapping algorithm consists in solving Eqs. (33)-(35) with respect to $\Delta\lambda$, A_{n+1} and $A_{\infty_{n+1}}$. Derivatives of Eqs. (33)-(35) with respect to unknowns $\{\Delta\lambda,\ A_{n+1},\ A_{\infty_{n+1}}\}$, as well as, the derivation of an analytical consistent tangent modulus can be found in (dos Santos et al., 2016a).

4 NUMERICAL EXAMPLES

This section is intended to assess the capabilities associated with the present model in accounting for high strain rate effects on material response: namely strain, strain rate hardening and viscous effects. By means of numerical simulations, local material response considering uniaxial tension/compression loading is analyzed. That is done by prescribing the value of axial strain E_{11} and associated strain rate $\bar{D}_{11}$. The material is elastic-viscoplastic and the corresponding material parameters are those given in Tab. 1, which were obtained by dos Santos et al. (2016b) considering available experiments related to an annealed OFHC copper (Tanner and McDowell, 1999; Nemat-Nasser and Li, 1998; Jordan et al., 2013). Classical relationships relate the *Young* modulus E and *Poisson* ratio ν appearing in Tab. 1 with elastic coefficients μ and κ of Eq. (4) through $\mu = \frac{E}{2(1+\nu)}$ and $\kappa = \frac{E}{3(1-2\nu)}$.

4.1 Decremental strain rate test

In a decremental strain rate testing, material is subjected to a monotonic high loading with a given high strain rate $\bar{D}_{11_1}$, which is then abruptly decreased to a value $\bar{D}_{11_2}$. Strain rate hardening phenomenon is evidenced when the decremental response is compared to that obtained during a constant strain rate $\left(\bar{D}_{11} = \bar{D}_{11_2}\right)$ monotonic loading. In order to simulate this test, subsequent analysis considers two load conditions (employed in experiments performed by Tanner and McDowell (1999)): (i) *a quasi-static* test (Q-S), in which the material is subjected to a total strain equal to 92% imposed very slowly with $\bar{D}_{11} = 4\times10^{-4}\,\mathrm{s}^{-1}$; (ii) a *decremental strain rate* test (DSR), where the material is subjected to at a high strain rate of $\bar{D}_{11_1} = 6\times10^{3}\,\mathrm{s}^{-1}$ until a partial strain of 32% is reached, and then the strain rate is abruptly changed to a lower value $\bar{D}_{11_2} = 4\times10^{-4}\,\mathrm{s}^{-1}$ while strain reaches 79%.

Numerical analyzes were performed considering a local convergence tolerance equal to 10^{-6}, 92 time steps[3] for *Q-S* simulation and 78 for the *DSR* case. Numerical results are showed in Figs. 2(a) and (b), which demonstrate the strain rate hardening effects on material response. A good agreement between model prediction and experimental results is observed in Fig. 2(a), where theoretical stress-strain curves for *Q-S* and *DSR* results are compared with experiments

[3]Numbers of time steps are equal to number of experimental points.

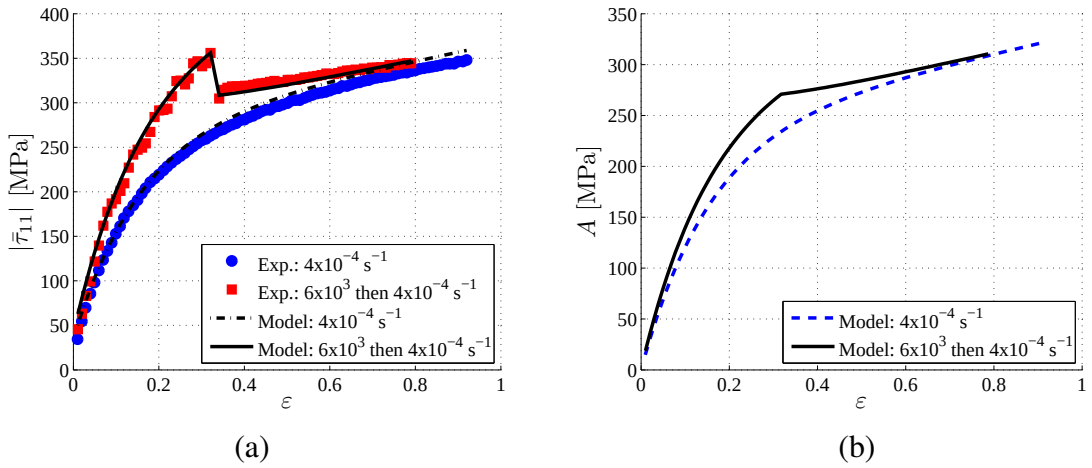

Figure 2: Decremental strain rate test results: (a) Model-predicted stress-strain curves compared with experimental data of Tanner and McDowell (1999); (b) Stress hardening vs. accumulated viscoplastic strain curves.

of Tanner and McDowell (1999). A sharp flow stress decreasing is observed when the strain rate changes instantaneously from $\bar{D}_{11_1} = 6 \times 10^3\,\mathrm{s}^{-1}$ to $\bar{D}_{11_2} = 4 \times 10^{-4}\,\mathrm{s}^{-1}$. This behavior evidences the instantaneous rate-sensitivity associated with viscous deformation mechanisms. In contrast, no jump is observed in hardening response as illustrated by Fig. 2(b). This feature could be expected, once the hardening response is related to current microstructural state, which does not undergo an instantaneous change by abruptly shifting the imposed strain rate (see, e.g., Klepaczko (1975) and Rashid et al. (1992)). Moreover, both stress and hardening responses of *DSR* simulation show an asymptotic tendency to the monotonic loading curve *Q-S*, what is the resulting strain rate history effect, not only on hardening, but also on the flow stress response. A higher previous strain rate induces a larger hardening when compared to a lower strain rate imposed during the whole deformation process. This behavior can be attributed to strong microstructural rate-dependence associated with FCC metals (Klepaczko, 1975; Chiem and Duffy, 1983; Klepaczko and Chiem, 1986; Rashid et al., 1992). Reasoning on modeling aspects, the present formulation is able of capturing stain-rate-induced hardening by means of the rate-sensitivity attributed to the saturation parameter A_∞ (see Eq. (15)).

Table 2: Loading strain rates of stress relaxation testing.

	Q-S	*Case 1*	*Case 2*	*Case 3*
$\bar{D}_{11}$ $[\mathrm{s}^{-1}]$	4×10^{-4}	10^3	6×10^3	9×10^3

4.2 Constant strain rate loading and stress relaxation testing

Strain rate hardening can also be characterized from stress relaxation testing, where the obtained equilibrium state reflects the current microstructural configuration. Therefore, the strain rate history effects on material state can be evaluated by varying the loading rate preceding stress relaxation, and thus observing the equilibrium stress states reached asymptotically. A

constitutive model capable of accounting for strain rate history effects should be able of predicting the distinct equilibrium stress states reached after different previous loading rates. For this purpose, numerical simulations of stress relaxation tests are undertaken using the present viscoplastic formulation.

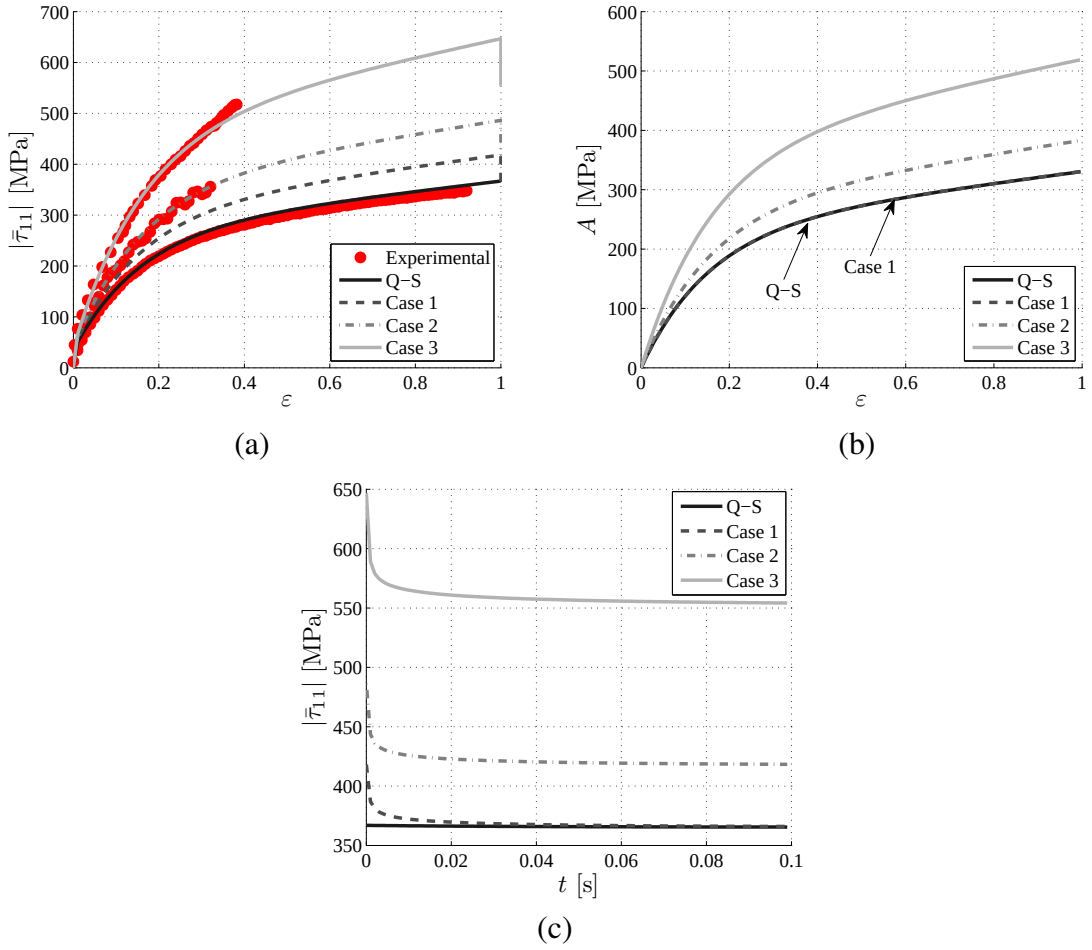

Figure 3: (a) Strain rate effects on stress-strain curves: comparison of model prediction and experiments of Tanner and McDowell (1999) (*Q-S* and *Case 2*) and Jordan et al. (2013) (*Case 3*); (b) Strain rate history effect on hardening curves; (c) Strain rate history effect on stress relaxation.

The numerical analyzes are carried out prescribing a total strain equal to 100% at different strain rates (see Tab. 2) and then keeping it constant along time. The material properties are those given in Tab. 1. All analyzes were performed considering 200 time steps and a local convergence tolerance equal to 10^{-6}. The stress-strain curves obtained for loading and stress relaxation simulations are showed in Fig. 3(a). In this figure, *Q-S*, *Case 2* and *Case 3* results are compared with experiments showing a good agreement. As expected, the flow stress is an increasing function of strain rate. This effect could readily be predicted by a conventional viscoplastic model that accounts only for instantaneous rate-sensitivity. However, the proposed constitutive model is also capable to predict the hardening rate-sensitivity.

Here, the hardening variable A increases with rate $\dot{\varepsilon}$, as emphasized in Fig. 3(b). But, the strain rate influence on hardening becomes more pronounced only for strain rates exceeding $10^3\,\mathrm{s}^{-1}$. That is, up to a strain rate of $10^3\,\mathrm{s}^{-1}$ (*Q-S* and *Case 1*) hardening responses are practi-

cally rate-independent, and for strain rates greater than $10^3\,\mathrm{s}^{-1}$ (*Case 2* and *Case 3*) the effect of previous loading rate on hardening variable A becomes significant. The rate dependence of A can also be clearly evidenced in Fig. 3(c)[4], where the relaxation response tends toward an asymptotic equilibrium stress state, which is given by the strength $(\sigma_y + A)$ associated with each previous loading rate. In Fig. 3(c), the curve associated with *Case 1* curve reaches the *Q-S* response asymptotically, demonstrating that the difference between the *Q-S* and *Case 1* results observed in Fig. 3(a) is mainly due to instantaneous rate-sensitivity. On the other hand, the equilibrium stress state $(\sigma_y + A)$ is significantly increased by strain rate for values exceeding $10^3\,\mathrm{s}^{-1}$.

5 CONCLUSIONS

Continuum and numerical viscoplastic formulations to model macroscopic strain rate history effects were formulated. Constitutive capabilities associated with present approach were assessed by means of homogeneous decremental strain rate and constant strain rate loading followed by stress relaxation testing. Numerical results have demonstrated the model aptitude to properly describe the main features of high strain rate loading on viscoplastic material response. In general, numerical results obtained in this paper, demonstrating good correlation with experimental data, contribute to the understanding of high velocity deformation processes and encourage future researches on the high strain rate behavior of metallic materials.

ACKNOWLEDGEMENTS

The author Tiago dos Santos wishes to acknowledge the doctoral scholarship support of *CAPES*, Coordenação de Aperfeiçoamento de Pessoal de Nível Superior of Brazil. Process number BEX 7023/15-4. The author Rodrigo Rossi wishes to acknowledge the support of *CNPq*, Conselho Nacional de Desenvolvimento Científico e Tecnológico of Brazil. Grant number 302605/2012-6 and 304044/2015-6.

REFERENCES

Anand, L., 1985. Constitutive equations for hot-working of metals. *International Journal of Plasticity*, vol. 1, n. 3, pp. 213 – 231.

Bodner, S. R. & Rubin, M. B., 1994. Modeling of hardening at very high strain rates. *Journal of Applied Physics*, vol. 76, n. 5, pp. 2742–2747.

Chiem, C. & Duffy, J., 1983. Strain rate history effects and observations of dislocation substructure in aluminum single crystals following dynamic deformation. *Materials Science and Engineering*, vol. 57, n. 2, pp. 233–247.

Coleman, B. D. & Gurtin, M. E., 1967. Thermodynamics with Internal State Variables. *Reports on Progress in Physics*, vol. 47, pp. 597–613.

de Souza Neto, E. A., Perić, D., & Owen, D. R. J., 2008. *Computational Methods for Plasticity: Theory and Applications*. John Wiley & Sons.

[4]The reference time $t = 0$ of Fig. 3(c) corresponds to the beginning of stress relaxation phase.

dos Santos, T., Rosa, P. A., Maghous, S., & Rossi, R., 2016a. A numerical viscoplastic model for strain, strain rate hardening, and viscous effects in cold deformation of polycrystalline FCC metals. *Submmited to International Journal of Mechanical Sciences*, vol. , pp. XX–XX.

dos Santos, T., Rosa, P. A., Maghous, S., & Rossi, R., 2016b. A simplified approach to high strain rate effects in cold deformation of polycrystalline FCC metals: Constitutive formulation and model calibration. *International Journal of Plasticity*, vol. , pp. (In press).

Durrenberger, L., Molinari, A., & Rusinek, A., 2008. Internal variable modeling of the high strain-rate behavior of metals with applications to multiphase steels. *Materials Science and Engineering: A*, vol. 478, n. 1-2, pp. 297 – 304.

Eterovic, A. L. & Bathe, K.-J., 1990. A hyperelastic-based large strain elasto-plastic constitutive formulation with combined isotropic-kinematic hardening using the logarithmic stress and strain measures. *International Journal for Numerical Methods in Engineering*, vol. 30, n. 6, pp. 1099–1114.

Follansbee, P. & Kocks, U., 1988. A constitutive description of the deformation of copper based on the use of the mechanical threshold stress as an internal state variable. *Acta Metallurgica*, vol. 36, n. 1, pp. 81 – 93.

Gao, C. & Zhang, L., 2012. Constitutive modelling of plasticity of fcc metals under extremely high strain rates. *International Journal of Plasticity*, vol. 32-33, n. 0, pp. 121 – 133.

Huang, F. & Tao, N., 2011. Effects of strain rate and deformation temperature on microstructures and hardness in plastically deformed pure aluminum. *Journal of Materials Science & Technology*, vol. 27, n. 1, pp. 1–7.

Jordan, J., Siviour, C., Sunny, G., Bramlette, C., & Spowart, J., 2013. Strain rate-dependant mechanical properties of ofhc copper. *Journal of Materials Science*, vol. 48, n. 20, pp. 7134–7141.

Klepaczko, J., 1975. Thermally activated flow and strain rate history effects for some polycrystalline f.c.c. metals. *Materials Science and Engineering*, vol. 18, n. 1, pp. 121 – 135.

Klepaczko, J. & Chiem, C., 1986. On rate sensitivity of f.c.c. metals, instantaneous rate sensitivity and rate sensitivity of strain hardening. *Journal of the Mechanics and Physics of Solids*, vol. 34, n. 1, pp. 29–54.

Klepaczko, J. R., 1988. Constitutive modeling in dynamic plasticity based on physical state variables - a review. *J. Phys. Colloques*, vol. 49, pp. 553–560.

Lee, E. H., 1969. Elastic-plastic deformation at finite strains. *Journal of Applied Mechanics*, vol. 36, pp. 1–6.

Lubliner, J., 1972. On the thermodynamic foundations of non-linear solid mechanics. *International Journal of Non-Linear Mechanics*, vol. 7, n. 3, pp. 237–254.

Lubliner, J., 1984. A maximum-dissipation principle in generalized plasticity. *Acta Mechanica*, vol. 52, pp. 225–237.

Luo, Z., Zhang, H., Hansen, N., & Lu, K., 2012. Quantification of the microstructures of high purity nickel subjected to dynamic plastic deformation. *Acta Materialia*, vol. 60, n. 3, pp. 1322 – 1333.

Lush, A., Weber, G., & Anand, L., 1989. An implicit time-integration procedure for a set of internal variable constitutive equations for isotropic elasto-viscoplasticity. *International Journal of Plasticity*, vol. 5, n. 5, pp. 521 – 549.

Mandel, J., 1972. *Plasticité classique et viscoplasticité: course held at the Department of Mechanics of Solids, September-October, 1971*. Courses and lectures - International Centre for Mechanical Sciences. Springer-Verlag.

Mandel, J., 1973. Equations constitutives et directeurs dans les milieux plastiques et viscoplastiques. *International Journal of Solids and Structures*, vol. 9, n. 6, pp. 725–740.

Molinari, A. & Ravichandran, G., 2005. Constitutive modeling of high-strain-rate deformation in metals based on the evolution of an effective microstructural length. *Mechanics of Materials*, vol. 37, n. 7, pp. 737 – 752.

Mourad, H., Bronkhorst, C., Addessio, F., Cady, C., Brown, D., Chen, S., & Gray, George T., I., 2014. Incrementally objective implicit integration of hypoelastic-viscoplastic constitutive equations based on the mechanical threshold strength model. *Computational Mechanics*, vol. 53, n. 5, pp. 941–955.

Nemat-Nasser, S. & Li, Y., 1998. Flow stress of f.c.c. polycrystals with application to OFHC Cu. *Acta Materialia*, vol. 46, n. 2, pp. 565–577.

Perić, D., 1993. On a class of constitutive equations in viscoplasticity: Formulation and computational issues. *International Journal for Numerical Methods in Engineering*, vol. 36, n. 8, pp. 1365–1393.

Perzyna, P., 1966. Fundamental problems in viscoplasticity. volume 9 of *Advances in Applied Mechanics*, pp. 243–377. Elsevier.

Perzyna, P., 1971. Thermodynamic theory of viscoplasticity. volume 11 of *Advances in Applied Mechanics*, pp. 313–354. Elsevier.

Rashid, M. M., Gray, G. T., & Nemat-Nasser, S., 1992. Heterogeneous deformations in copper single crystals at high and low strain rates. *Philosophical Magazine A*, vol. 65, n. 3, pp. 707–735.

Rice, J., 1971. Inelastic constitutive relations for solids: An internal-variable theory and its application to metal plasticity. *Journal of Mechanics Physics of Solids*, vol. 19, pp. 433–455.

Rodríguez-Martínez, J., Rodríguez-Millán, M., Rusinek, A., & Arias, A., 2011. A dislocation-based constitutive description for modeling the behavior of {FCC} metals within wide ranges of strain rate and temperature. *Mechanics of Materials*, vol. 43, n. 12, pp. 901 – 912.

Rodríguez-Martínez, J., Rusinek, A., & Klepaczko, J., 2009. Constitutive relation for steels approximating quasi-static and intermediate strain rates at large deformations. *Mechanics Research Communications*, vol. 36, n. 4, pp. 419 – 427.

Rusinek, A. & Jankowiak, T., 2014. *Constitutive Relations under Impact Loadings: Experiments, Theoretical and Numerical Aspects*, chapter Dynamic Behavior of Materials. Constitutive Relations and Applications, pp. 87–135. Springer Vienna, Vienna.

Rusinek, A. & Klepaczko, J., 2001. Shear testing of a sheet steel at wide range of strain rates and a constitutive relation with strain-rate and temperature dependence of the flow stress. *International Journal of Plasticity*, vol. 17, n. 1, pp. 87 – 115.

Simo, J. C. & Hughes, T. J. R., 1998. *Computational Inelasticity*. Interdisciplinary applied mathematics: Mechanics and materials. Springer.

Tanner, A. B. & McDowell, D. L., 1999. Deformation, temperature and strain rate sequence experiments on {OFHC} {Cu}. *International Journal of Plasticity*, vol. 15, n. 4, pp. 375–399.

Voce, E., 1948. The relationship between stress and strain for homogeneous deformation. *Journal of Institute of Metals*, vol. 74, pp. 537–562.

Voyiadjis, G. Z. & Almasri, A. H., 2008. A physically based constitutive model for fcc metals with applications to dynamic hardness. *Mechanics of Materials*, vol. 40, n. 6, pp. 549 – 563.

Wang, W. M., Sluys, L. J., & de Borst, R., 1997. Viscoplasticity for instabilities due to strain softening and strain-rate softening. *International Journal for Numerical Methods in Engineering*, vol. 40, n. 20, pp. 3839–3864.

Weber, G. & Anand, L., 1990. Finite deformation constitutive equations and a time integration procedure for isotropic, hyperelastic-viscoplastic solids. *Computer Methods in Applied Mechanics and Engineering*, vol. 79, n. 2, pp. 173–202.

Zaera, R. & Fernández-Sáez, J., 2006. An implicit consistent algorithm for the integration of thermoviscoplastic constitutive equations in adiabatic conditions and finite deformations. *International Journal of Solids and Structures*, vol. 43, n. 6, pp. 1594 – 1612.